Analytical Methods

Paper

Fluorescent microRNA Biosensors: A comparison of signal generation to quenching

C. Kyle Almlie[a], Nicholas E. Larkey[a], and Sean M. Burrows*[a]

Many microRNA biosensor platforms use fluorescence signal generation or quenching; however, signal generation is often regarded as the superior method. An argument can be made that if the noise is the same for both methods, then there should be no difference between the two methods. Current literature details the analytical figures of merit (FOM) for transduction and recognition mechanisms that use either signal generation or quenching, but lacks a direct comparison using the same fluorescent reporter molecule. Here we provide such a direct comparison. The signal-on and signal-off fluorescence metrics were found to be comparable rather than competitive. We found fluorescence enhancement provides marginal improvements to sensitivity and limits of detection (LOD) over fluorescence quenching. In fact, both transduction mechanisms are capable of picomolar LOD. The role thermodynamics plays on the sensitivity and LOD are discussed. Both signal-on and signal-off gave statistically similar signal-to-noise ratios. Finally, the selectivity of the two recognition mechanisms for miRNA detection will be addressed. In the future, we will use this knowledge to advance highly sensitive and selective *in situ* microRNA sensors for cell and tissue imaging.

Analytical Methods

Paper

Introduction

The growing understanding of the role that microRNA (miRNA) plays in post-transcriptional gene regulation has led to an increased demand for sensitive and selective biosensors that can withstand or mitigate enzymatic degradation and off-target interactions.[1–6] There are many fluorescent nucleic acid biosensor platforms for RNA/DNA analysis in cells and tissues.[7–22] In general, there are two mechanisms fluorescent biosensors use to achieve a change in signal: either signal generation (signal-on)[10–12] or signal quenching (signal-off).[13–15]

Fluorescence generation is often regarded as more sensitive than quenching mechanisms because conceptually it is easier to detect a signal increase from a dark background as opposed to detecting a decrease from a bright signal. Such an argument is typically used to explain why fluorescence is regarded as having better sensitivity than absorbance.[23] However, one could argue that if the noise is identical for signal-on and -off, then the sensitivity and limits of detection should be the same.

There are many analytical figures of merit (FOM) that need to be considered in order to gauge a biosensor's attributes. The overall performance of a biosensor can be determined from sensitivity, selectivity, limits of detection and quantitation (LOD and LOQ), signal-to-noise ratio (S/N), signal-to-background ratio, kinetics, false signal generation, accuracy, and reproducibility.[1,5]

There is no perfect nucleic acid biosensor that will optimize all of the analytical FOM; however, there are several that have varying degrees of advantages and disadvantages. When attempting to determine if signal-on really is superior to signal-off, the specific application must be considered as well as the FOM of the biosensor. Some biosensors utilize signal-on methods for improved sensitivity at the expense of another analytical FOM. Conversely, a signal-off method may prove to have moderate sensitivity but improve other important FOMs.

Evaluation of the current literature concerning nucleic acid biosensors reveals the trade-off between analytical FOM's for signal-on and signal-off. Silver nanoclusters have been found to be highly selective and easily multiplexed, but lack sensitivity and robustness.[14,16] Molecular beacons based on organic quenching dyes or gold nanoparticles boast high selectivity and sensitivity, but are susceptible to false signal generation from degradation and in some cases poor selectivity.[8]

One method of increasing sensitivity involves improving quenching mechanisms to reduce the background fluorescence prior to analyte binding.[11,12,15,18,24,25] Recent work with graphene oxide based quenchers has shown high selectivity (90 %) for miR-16, miR-21, and miR-26a. However, this comes at a cost of increased time for analysis and undesired side reactions from amplification procedures.[11,15] Du *et al.* have demonstrated the use of gold nanoparticles as efficient quenchers that are combined with a molecular beacon-like transduction mechanism to gain single-mismatch selectivity.[24] Unfortunately, the surface-immobilized sensor design is complicated by additional preparation procedures for coating the nanoparticles as well as requiring rinsing steps.

Furthermore, their biosensor suffers from poor sensitivity below a target concentration of 2 μM and a non-linear response above 2 μM. Work with Cadmium quantum dots in a Förster Resonance Energy Transfer (FRET)-quenching signal-off mechanism has shown great sensitivity (1 fM for miRNA-21) and selectivity (~ 50% for single-mismatch miRNA-21).[13] The downside is the unavoidable toxicity of Cadmium that limits the *in vivo* applications of the biosensor.

The difference between signal-on and signal-off methods is well recognized. Some current literature seeks to work around the pros and cons of both signal-on and signal-off. For example, Kang *et al.* describe a dual biosensing system to overcome the deficiencies of signal-on and signal-off.[17] They used a luciferase assay in signal-off mode upon binding of target analyte and a molecular beacon in signal-on mode for the same target analyte. While the dual sensing system employs both a signal-on and a signal-off method, both the transduction and recognition mechanisms are different and thus a direct comparison of signal-on and signal-off analytical FOM cannot be made.

Other work seeks to use signal-on and signal-off as a type of molecular opened/closed indicator. Landon *et al.* reported the use of DNA zippers and tweezers that alter the proximity of a fluorescent dye and quencher in the presence of various opening and closing strands.[26] The authors did not compare the sensitivity of signal-on to signal-off. However, they did demonstrate that DNA zippers have selectivity for the target strand in the presence of non-complementary strands with up to 24 % sequence mismatches.

All biosensors have distinct advantages and disadvantages depending on the specific application. However, of the literature we could find, none of the methods have directly evaluated analytical FOM for both signal-on and -off with the same fluorescent reporter molecule. Therefore, it is difficult to compare fluorescent enhancement or quenching analytical FOM for two separate reporting molecules, since they will always have some benefits and pitfalls that will favor one figure of merit over another. A direct comparison of the difference between signal-on and signal-off should be done with two biosensors that use the same reporting molecules and have closely related recognition mechanisms.

We have recently created a fluorescent miRNA-biosensor that mitigates false signal generation and has shown rapid and selective detection of let-7a with nanomolar detection limits.[1] Our 'reporter-probe' biosensor consists of a Cy3/Cy5 dye pair on a self-complementary reporter oligonucleotide strand that partially binds to a probe sequence. Competitive binding of miRNA analyte, let-7a, for probe (P) displaces the reporter from the reporter-probe complex (RQ+P). False signal reduction was achieved because the reporter brings two dyes together after displacement from the reporter-probe complex. The competitive displacement reaction operates at a user-defined temperature to control the selectivity of the reporter-probe biosensor. This is in contrast to other biosensors that

Table 1. Oligonucleotide Sequences ^{a}

Name:	Sequence (5' - 3'):
RQ	5Cy5/<u>CATCG</u>TTGAATAC+***TAGGTTGT***+***ATAGT***T<u>CGAT+G</u>/3IAbRQSp
Probe	***ACTATACAACCTA***CTACCTC
Let-7a	T**GAGGTAGTAGGTTGTATAGT**T
RT	**AACTATACAACCTAGTATTCA**
MB	5Cy5/<u>TCATCG</u>**AACTATACA+ACCTACTAC+CTCA**<u>CGAT+GA</u>/3IAbRQSp
Let-7aV^b	**U*GA*uGUA**ca**AGGUUGUAU*AGU*U**

^{a} Bold sections refer to complementary binding sites. Bold and italic show where the reporter and probe hybridize. Underlined sections depict complementary regions of the stems for RQ and MB. (+) symbol represents location of locked nucleic acid. (*) symbol represents location of a phosphorothioated modification. ^{b} Let-7aV was purchased as RNA. The lowercase letters in let-7aV show the position of the nucleotides that were changed relative to let-7a.

require a temperature gradient to impart selectivity.[8,10]

The way in which the reporter folded into a hairpin leads to ~ 50 % quenching of the Cy5 emission. The work presented here uses the same reporter-probe recognition mechanism but uses a Cy5 and Iowa Black Red Quencher on distal ends of the reporter (referred to as RQ for Reporter-Quencher). The use of a quencher resulted in ~ 80 % reduction of the Cy5 signal.

Here we directly compare and contrast the analytical FOM of fluorescence generation and quenching using the same reporter molecule. The analytical FOM of interest are: sensitivity, selectivity, limits of detection and quantitation (LOD and LOQ), reproducibility, accuracy, precision, and signal-to-noise ratio (S/N). Signal-on and -off were addressed using a reporting strand with the same reporting fluorophore, quencher, and nucleic acid sequence. For signal-on, the loop region of the reporter strand was capable of binding to either a partially complementary probe (P) or a fully complementary reporter target (RT). The RT helps ensure that the analytical FOM determined for signal-on account for the complementarity of the binding. For signal-off, the probe binds the analyte with full complementarity. Displacement of the reporter causes the signal to decrease as it refolds into the hairpin conformation. Using this approach the analytical FOM are representative of the transduction mechanism.

To compare the analytical FOM for the same miRNA analyte, let-7a, we designed a molecular beacon (MB). The MB was similar to the reporter in terms of the stem sequence and fluorophore-quencher pair, but the loop region was changed to be complementary for let-7a. A terminal Adenine-Thymine base pair was added to the stem of the MB to improve the stability and ultimately the selectivity. We will show the sensitivity of signal-on is only a factor of 1 to 2 greater than signal-off. The limits of detection and quantitation were over a factor of 20 better for signal-on than signal-off. We will demonstrate that the signal-to-noise ratio was comparable for both methods. Finally, we will show the selectivity of the reporter-probe biosensor was superior to the molecular beacon.

Experimental

Recognition and Transduction Mechanism

Several analytical FOM for signal-on were directly compared to those for signal-off using the same reporter molecule. These merits include detection limits, sensitivity, selectivity, signal-to-noise, reproducibility, accuracy, and precision. The analytical FOM for detection of let-7a were compared between the (RQ+P) biosensor and a molecular beacon. All sequences used are listed in Table 1. DNA was
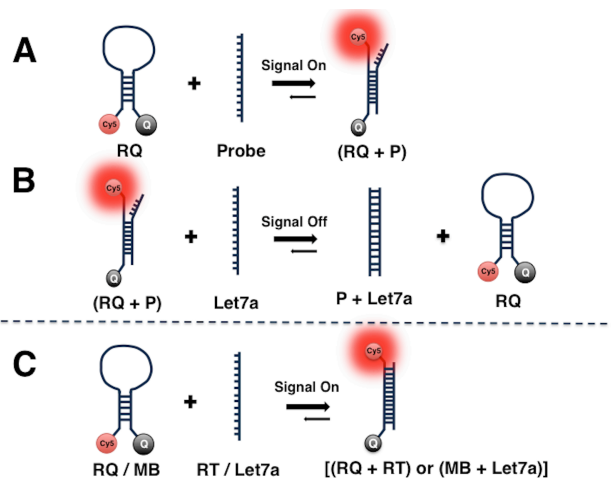
Scheme 1. Recognition and Transduction Mechanisms: (A) RQ with added probe turns the signal-on. (B) The reporter – probe complex with addition of the let-7a target turns the signal-off as the probe – target complex is formed. (C) Signal-on with (RQ+RT) or (MB+let-7a). Note that RT and let-7a have different sequences but are fully complementary to their respective reporter or MB loop sequence. The secondary structure of the RQ hairpin is a generic representation of a hairpin and is not representative of the true secondary structure. A more accurate illustration of the RQ hairpin is included in Figure 4.

used instead of miRNA because it is more stable and thus easier to work with.

The RQ starts in a hairpin conformation where the quencher is next to Cy5, minimizing emission from Cy5 (Scheme 1A). As probe binds to the loop region of RQ the hairpin opens, moving the quencher away from the Cy5 dye, allowing for an increase in fluorescence emission. The reporter-probe complex (RQ+P) was then used to evaluate the analytical FOM for signal-off. The parentheses around the RQ and P signify that they are bound together as the complex. Signal-off was achieved by increasing target analyte (a DNA mimic of let-7a miRNA) concentration in the presence of the reporter-probe complex (Scheme 1B). Addition of target analyte causes the probe to form a more thermodynamically stable complex with the miRNA analyte and displaces the reporter. This process allows the reporter to return to the hairpin and quench the Cy5 emission (Scheme 1B).

Since the probe is only partially complementary to the loop region of the reporter, there was concern over how the amount of complementarity between the reporter and probe would influence the analytical figures of merit. To address this issue a target sequence that was fully complementary to the loop region

of the reporter, RT, was designed and tested (Scheme 1C). In this case RQ was used like a molecular beacon for signal generation. These experiments allowed comparison of signal-on to signal-off using the same molecular structure of reporter molecule. However, this did not compare FOM for the same target.

In order to compare analytical figures of merit for the same target a molecular beacon (MB) for let-7a was designed. The MB had the same Cy5 dye and quencher (Scheme 1C) as the reporter. The stems of the MB and RQ were also similar, except MB has an additional terminal Adenine-Thymine base pair to improve selectivity. Selectivity in terms of non-specific binding was determined for (RQ+P) complex and MB using let-7aV, a tri-nucleotide variant of let-7a. See Table 1 for a list of all nucleic acid sequences used in this study.

Signal Acquisition

All spectra were collected with a custom-built fluorimeter detailed in previous work.[1] Briefly, a Titanium-Sapphire laser (Mai Tai, Spectra Physics, Newport Corporation) tuned to emit 742 nm of pulsed light was used as the excitation source (100 femtosecond pulses, 80 MHz repetition rate). The average power was selected using a half-waveplate and polarizing beam splitter. The angle of the half-waveplate's optical axis was set using a computerized controller (Newport Corporation). All experiments were conducted at an average power of approximately 75 mW. Fluorescence was collected using the same lens for excitation and separated from the incident beam using a 705 nm long pass dichroic mirror (Semrock, FF705-Di01-25x36). Backscatter from the laser into the spectrometer was minimized using a 720 nm shortpass filter (Semrock, FF01-720/SP-25). The signal then entered the back of an objective (10x, 0.25 NA) for fiber optic coupling. The fiber optic delivered the signal to an Acton Spectrometer (SP-2356, 300 mm focal length, Princeton Instruments) equipped with a 300 groove/mm grating blazed at 500 nm. The grating center wavelength was set to 680 nm to correspond with the Cy5 emission peak. To allow maximum light throughput, the entrance slit was opened to 1 000 μm. Signal was acquired with an electron multiplied CCD detector (512B-eX-celon3-EMCCD, Princeton). Acquisition settings were optimized for different RQ concentrations. For analysis starting with 1 μM RQ with 500 nM probe (500 nM (RQ+P) complex and 500 nM RQ), 500 nM (RQ+P) complex, 1 μM MB, or 500 nM MB; the detector was set to: 100 ms exposure time, 10 exposures averaged per frame, 6 frames were collected to gauge instrumental error, 600 ns frame transfer read-out mode, a region of interest (ROI) of 512 x 17 (4 vertical rows binned), high Analog-to-Digital Conversion gain (ADC), 5 MHz ADC speed, and the CCD was thermoelectrically cooled to -70 °C to minimize dark noise. For 1 nM RQ, Electron Multiplied (EM) Gain mode was used with 75x gain, 1 000 ms exposure time averaging 20 exposures per frame with 6 frames saved per file. All other parameters were the same as for the micromolar solutions. To gauge error from cuvette placement all samples were subjected to three cuvette placements. A cuvette placement consisted of lifting the cuvette from the holder and replacing it prior to the next measurement. Cuvette error analysis was needed because of the custom nature of the fluorimeter. Commercial systems with a locking position cuvette holder would not need such error analysis.

Solution Preparation

All oligonucleotide strand sequences in Table 1 were purchased from IDT (Integrated DNA Technologies, Inc., Coralville, Iowa, United States). Tris buffer (pH 10), Tween-20, phosphate buffered saline (PBS 1X, pH 7.0), and 2 M magnesium chloride ($MgCl_2$) were obtained from Fisher Scientific and used as received. Working solutions of oligonucleotides were prepared by diluting stock oligonucleotide solutions in a custom buffer that consisted of: 10 mM Tris buffer (pH 10), 2.5 mM $MgCl_2$, and 0.005 % Tween-20 in PBS 1X. The final pH of the solution was around 8. All work was done at room temperature (~ 22 °C).

Signal-on analytical FOM were investigated by preparing solutions of 1 μM RQ with incremental additions of 100 nM to 750 nM probe (P) or reporter target (RT). The solutions were allowed to hybridize for 20 minutes.

Signal-off figures of merit were acquired by first incubating RQ and P at a 2:1 ratio (1 μM RQ : 0.5 μM P) for 20 minutes to ensure all P was bound for a final (RQ+P) complex concentration of 500 nM. The unbound RQ remained in the hairpin conformation, but due to insufficient quenching there was a small amount of background fluorescence (see supplemental Figure S1). Next, increasing amounts of let-7a analyte from 100 nM to 750 nM were added to the (RQ+P) biosensor. All analyte additions were allowed to hybridize for 10 minutes. The RQ concentration was reduced to 1 nM with 500 pM P to make 500 pM (RQ+P) complex. This complex was titrated with let-7a from a concentration of 50 pM to 750 pM, using similar incubation times as before: 20 minutes to form the (RQ+P) complex, followed by 10 minutes after addition of let-7a.

A 3-nucleotide variant of let-7a (let-7aV) was used to test the selectivity of the (RQ+P) complex and MB. The (RQ+P) was prepared by hybridization of 500 nM RQ and 500 nM P for 20 minutes. The concentration of the MB was also 500 nM. Each solution was made separately to accommodate the addition of up to 500 nM let-7a or let-7aV with a 10 minute incubation time.

Solutions were prepared to examine inter- and intra-assay variability for signal-off. Intra-assay variability solutions were prepared as a series of increasing analyte concentrations using 3x the volume needed for one experiment. The solution at each analyte concentration was then aliquoted into three separate vials prior to analysis. Inter-assay solutions were prepared by making the series of increasing analyte concentrations with enough volume for one experiment. This process was repeated for a total of three times to determine day-to-day solution preparation variations.

Data Processing

All data was processed with a custom written MATLAB code (R2012b, The MathWorks, Inc., Natick, Massachusetts, United States). Each data point in the calibration curves was a background corrected sum from 640.1425 to 690.0957 nm over an averaged fluorescence peak (N = 3). Analyte, probe, and reporter concentrations were validated using a calibrated Nanodrop 1 000 spectrophotometer (Thermo Fisher Scientific, United States). The true concentration of analyte was taken as that determined by Nanodrop. Then the RQ, P, and let-7a concentrations were multiplied by a correction factor to properly correlate fluorescence intensity with the true concentration in solution. For each cuvette placement the S/N ratio was found by averaging the intensity from 6 frames at 673.206 nm, and dividing the average by the standard deviation

of the 6 frames. Each S/N ratio was then averaged over three cuvette placements.

Thermodynamic and Structure Predictions

Predictions of the Gibbs energy and melting temperatures of the various conformations of the biosensors were obtained using freeware available from the DINAMelt Web Server managed by The RNA Institute at SUNY-Albany.[27-29] The predicted values cannot incorporate added stability from chemical modifications or any deviation in stability from dye and quencher interactions or their interactions with the nucleotides. Rather the predictions remain valuable on a comparative basis.

DINAMelt prediction of energy values for single stranded hairpins and hybridization of two single strands uses partition functions that take into account all possible conformations and configurations of the constituents.[27-29] For example, when calculating the ΔG for the hybridization of the (RQ+P) complex from single strands of RQ and P, the calculation considers the partition functions of folded RQ and P, unfolded RQ and P, (RQ+RQ) and (P+P) homodimers, and (RQ+P) heterodimer. In other words, the predicted ΔG includes the equilibriums of all possible conformations and configurations present in the hybridization of RQ with P. The reader is encouraged to review the works by Zuker and co-workers for an in-depth description of the assumptions and characteristics of the DINAMelt freeware.[27-29]

For single stranded hairpins DINAMelt assumes no homodimers will form. This assumption is based in the fact that the unimolecular hairpin must first unfold to a less stable open conformation before forming a stabilizing dimer. Zuker and co-workers state that assuming single stranded hairpins do not form homodimers does not limit the partition functions and calculated energy values.[29]

The "Two State melting (hybridization)" function was used for double-strand hybridization calculations. The "Quikfold" function was used for hairpin calculations. Hybridization parameters for all calculations were: 22 °C, 10 mM Na^+, 2.5 mM Mg^{++}, and 1 μM oligonucleotide. The Quikfold function did not allow for definition of oligonucleotide concentration. All other parameters for both the Quikfold and Two State melting (hybridization) were left at the default values. Thermodynamic values for let-7aV hybridization were calculated as a DNA sequence instead of an RNA sequence because there was no RNA-DNA option.

The DINAMelt servers do not provide an overlay of the hairpin conformational structures and associated probabilities. To gain such information the RNAstructure Web Servers at the University of Rochester Medical Center were used.[30] To mimic physiological conditions, RNAstructure pre-defines the sodium concentration as 1 M and this value cannot be changed. The only parameters we defined were DNA rules and 22 °C; all other user-defined values were left at the default settings. The resulting energy values and structures were similar between the DINAMelt and RNAstructure servers, provided the same salt concentrations were used.

Results and Discussion

Sensitivity and Detection Limits for Signal-on and Signal-off

Sensitivity of the reporter, RQ, is correlated to the slope of a calibration curve with either increasing amounts of probe (P) or reporter-target (RT) added to the RQ. Similar calibration curves for the (RQ+P) and molecular beacon (MB) used incremental additions of target analyte, let-7a. As mentioned previously, P and RT additions to RQ only provide a signal-on reference point for comparison to signal-off with the (RQ+P) biosensor. The MB provides a comparison of the FOM to (RQ+P) for the same analyte.

Figure 1 shows the sensitivity for signal-on using the RQ and MB plus their respective targets. The MB demonstrated the greatest sensitivity for let-7a, followed by the RQ for RT and then RQ for P. Figure 1, Figure 2, and Table 2 reveal that the sensitivity of signal-on with (RQ+P) and (RQ+RT) were only marginally better than signal-off by a factor of about 1.2 and 1.7, respectively. From Table 2 it is apparent this difference is small but statistically significant (95% confidence level).

Comparing the results of the RQ in Figure 2 to Table 2 for signal-on and signal-off show a small yet statistically significant discrepancy in the slopes. In the signal-on case, the sensitivity was 41 116 ± 2 347 for 1 μM RQ and 46 108 ± 1 511 counts/nM for 500 nM RQ. The same can be seen in the signal-off case, the sensitivity changes from -34 764 ± 4 331 to -38 587 ± 1 079 counts/nM, for the 1 μM RQ and 500 nM RQ, respectively. For the signal-off case it should be noted that both Figure 2 and Table 2 deal with 500 nM (RQ+P) complex, but in Table 2 there was an excess of 500 nM RQ that Figure 2 did not have. We attribute these increases in sensitivity to a lower background signal for the signal-on and signal-off case. In both cases there is a decrease in signal due to fewer fluorescent dyes in the detection volume at the lower concentrations of RQ. The fact that the sensitivity increased when fewer dye molecules were in the detection volume supports the hypothesis that it is easier to detect an increase or decrease in fluorescence when the background is dimmer.

Figure S1 helps visualize the lower signal for RQ at different concentrations. The reason uncomplexed RQ-hairpin contributes to the background signal is because the fluorescence is only 80 % quenched when in the hairpin conformation for a 1 μM solution. The remaining 20 % represents unquenched signal that contributes to the background signal. The 20 % unquenched signal comes from incomplete quenching by the Iowa Black Red Quencher and the fact that some hairpins are not fully closed and are in an open state. The spatial orientation

Table 2. Analytical Figures of Merit for Signal-on and -off

	Signal-on [a]			Signal-off [b]
	RQ + P	RQ + RT	MB + Let-7a	(RQ+P) + Let-7a
LOD (nM)	0.183 ± 0.117	0.098 ± 0.028	0.131 ± 0.036	2.72 ± 1.33
LOQ (nM)	0.609 ± 0.390	0.326 ± 0.094	0.437 ± 0.120	9.07 ± 4.44
RSD	63.9 %	28.8 %	27.6 %	50.0 %
Slope (counts/nM)	41116 ± 2347	60405 ± 1592	68804 ± 2627	-34764 ± 4331
RSD slope	5.7 %	2.6 %	3.8 %	12.5 %

[a] N = 3 , [b] N = 9 , RQ and MB at 1 μM. (RQ+P) at 500 nM with 500 nM excess RQ. Errors in slope, LOD, and LOQ for signal-on are all statistically similar
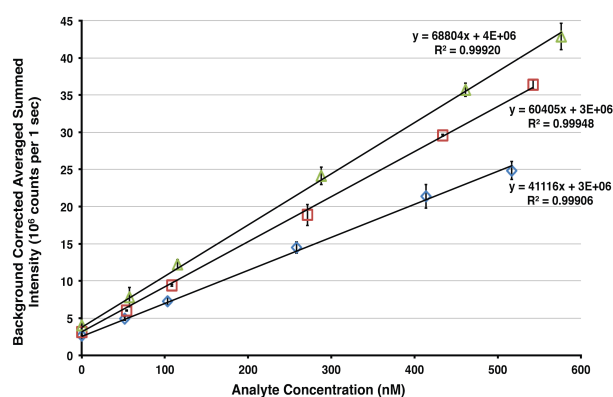
Figure 1. Comparison of slopes from titration of 1 μM RQ with either probe (blue diamonds) or RT (red squares). The green triangles are the titration of 1 μM MB with let-7a. The MB was the most sensitive followed by RQ+RT and RQ+P. Analyte concentrations were multiplied by an appropriate correction factor, obtained from Nanodrop, to account for slight variations in concentration from sample preparation. Error bars are the same size or smaller than the markers. Trend lines were forced through the zero analyte point. Scale 10^6 counts per 1 second.
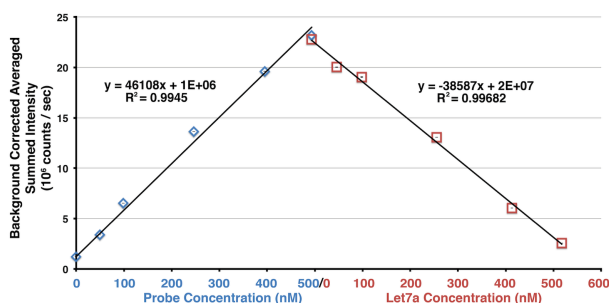

Figure 2. Titrations of 500 nM RQ with probe (blue diamonds) and 500 nM (RQ+P) complex with let-7a target (red squares). Analyte concentrations were multiplied by the Nanodrop determined correction factor to account for slight variations in concentration from sample preparation. Error bars are the same size or smaller than data markers. Trend lines were forced through their respective zero analyte points. Scale 10^6 counts per 1 second.

and distance between the quencher and Cy5 are important for both FRET and static quenching. If the hairpin does not fold in such a way to achieve optimal spatial distance and orientation, then the amount of quenching will suffer. The quenchers used in this study were obtained from IDT and optimized to quench fluorescence in the red region of the spectrum where Cy5 emits. Different stem sequences and use of spacers at the end of the stems will be explored in future work to obtain better quenching.

The average fluorescence from the RQ hairpin is an ensemble of various states of open and closed hairpins. The amount of hairpins that are in an open state was calculated from theoretical Gibbs energy values and the equilibrium constant for hairpin formation. Starting with 1 μM RQ gives an equilibrium concentration of about 2.6 nM of reporters remaining in some partially open conformation with the dyes further apart than when the hairpin is fully closed.

Sensitivity only reveals how much the signal will change per nanomolar analyte added. However, there is no information about statistically significant changes in concentration that will give statistically significant changes in signal. To make this

determination, limits of detection and quantitation were investigated.

The limits of detection were determined by taking three times the standard deviation of the signal intensity without analyte divided by the slope from the calibration data (data not shown, but similar to Figures 1 and 2). In this derivation the y-intercept was forced through the first data point (no analyte added). The limits of quantitation were determined with a similar method, but used 10 times the standard deviation of the signal intensity without analyte. The results are presented in Table 2 for comparison of signal-on to signal-off.

The signal-on LOD was assessed using three different analytes (P, RT, and let-7a) and two slightly different reporting molecules (RQ and MB). The only difference in reporting molecules was the sequence of the loop region. The LOD's for (MB+let-7a), (RQ+P), and (RQ+RT) were found to be statistically similar around 0.2 nM (at the 95 % confidence interval and N = 3). In comparison, the signal-on LOD of RQ for P and RT were respectively about 15 and 28 times more sensitive than the signal-off (RQ+P) biosensor. Upon comparison of LOD's for the same analyte (let-7a), the signal-on with the molecular beacon was about 21 times more sensitive than signal-off (RQ+P) biosensor.

The limits of detection of the signal-off biosensor were improved to the picomolar range by lowering the concentration of the (RQ+P) complex to 500 pM (1 nM RQ and 500 pM P). Titration of this (RQ+P) complex with let-7a target up to 500 pM gave an LOD and LOQ of 49.38 ± 1.77 pM and 164.60 ± 5.91 pM, respectively (data not shown, error represents cuvette placements from one experiment). These results show that by adjusting the reporter-probe concentration the limits of detection and dynamic range can be tuned.

While the signal-on mechanism showed high precision in the sensitivity (RSD Slope 3 to 6 %, Table 2), signal-off demonstrated moderately less precision with an RSD slope around 12 %. The precision is higher with the samples that were fully complementary (RQ + RT, MB + let-7a, ~ 3 % RSD), and there is less precision with the samples that have partial complementarity or competitive binding (RQ + P, (RQ+P) + let-7a, 6 and 12 % respectively). In terms of precision for LOD and LOQ, the fully complementary signal-on had the lowest RSD of about 28 % for both MB and RQ. The precision of the RQ for P and the (RQ+P) for let-7a were 64 and 50 %, respectively; a little more than twice that of the MB and RQ for their respective targets. This suggests that the precision of forming the (RQ+P) complex manifests itself in the precision for let-7a binding to the (RQ+P) biosensor.

Influence of Thermodynamic Parameters on Equilibrium Concentrations and Sensitivity

Figure 3 plots the Gibbs energy (ΔG, kcal/mol) and melting temperature (T_m, °C) of the various DNA structures involved in this study. The values were predicted from freeware available from The RNA Institute at SUNY-Albany.[27,28] DNA structures with negative Gibbs energy and melting temperatures over 22 °C (lab temperature) are considered stable. Greater stability is associated with larger negative Gibbs energy values and larger positive melting temperatures. Recall the thermodynamic values do not account for added stability of locked nucleic acids, dye-quencher interactions, or dye/quencher interactions with nucleic acids. As a result these values are most likely under or over estimates. However, the same chemical modifications, dyes, and quenchers were used allowing for a comparison of the thermodynamic values to evaluate the
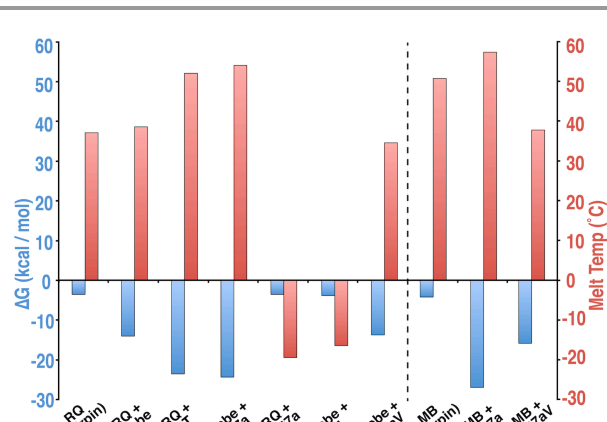
Figure 3. Predicted thermodynamic values demonstrate driving forces to form (RQ+P), subsequent (P+let-7a), and (MB+let-7a) complexes. The figure also helps compare selectivity of MB and (RQ+P) toward potential off-target interactions. The small ΔΔG between (RQ+P) and P+let-7aV is not enough to disrupt the complex, but the ΔΔG for the MB vs. (MB+let-7aV) competition is enough to open the MB. All values were obtained using freeware available from the DINAMelt Web Server managed by The RNA Institute at SUNY-Albany.[27-29]

relative stabilities of the various biosensor conformation and hybridization states. The thermodynamic values also allow for an estimation of equilibrium concentrations.

The stability of dimerization of two strands was defined as the change in Gibbs energy (ΔΔG) and the change in melting temperature (ΔT_m) before and after a hybridization reaction. The following equations were used to determine changes in thermodynamic values:

$$\Delta\Delta G = \Delta G_{final} - \Delta G_{initial} \qquad (1)$$

$$\Delta T_m = T_m^{final} - T_m^{initial} \qquad (2)$$

where final and initial represent the final and initial states of the hybridization reaction.

Table 3 lists the equilibrium constants, K_{eq}, and changes in melting temperature (ΔT_m) and Gibbs energy ($\Delta\Delta G$) upon target binding for the various biosensors. The changes in thermodynamic values are related to the thermodynamic driving force governing the change in equilibrium upon hybridization.

For the signal-on case there appears to be a relationship between the sensitivity and thermodynamic stability upon

Table 3. Predicted Equilibrium Constants and Change in Thermodynamic Values for Biosensing

Chemical Equilibrium	K_{EQ}*	$\Delta\Delta G$ (kcal/mol)	ΔT_m (°C)
MB+let-7a ⇌ (MB+let-7a)	8.3×10^{19}	- 23	+ 7
RQ+RT ⇌ (RQ+RT)	2.5×10^{17}	- 20	+ 15
RQ+P ⇌ (RQ+P)	2.3×10^{10}	- 11	+ 2
(RQ+P) + let-7a ⇌ RQ + (P+let-7a)	4.2×10^{7}	- 10	+ 16

* Units for equilibrium constants of bimolecular reactions that start with two reactants and produce one product will be 1/M but trimolecular reactions that involve a competition reaction of two reactants and give two products will have a unit-less equilibrium constant. The K_{EQ} for bimolecular reactions was determined using ΔG from DINAMelt. K_{EQ} for the trimolecular reaction uses K_{comp} derived in text.

comparison of Figure 1, Table 2, Figure 3, and Table 3. The order of most to least sensitive (i.e. the steepness of slopes) follows the thermodynamic stability in terms of ΔΔG and equilibrium constants for duplex formation from most to least stable: (MB+let-7a) > (RQ+RT) > (RQ+P), see Figure 3 and Table 3. Furthermore, the steeper slopes, greater stability, and larger equilibrium constants of (MB+let-7a) and (RQ+RT) compared to (RQ+P) reflect the fully complementary nature of the loop regions of the hairpins for their respective targets.

In general, the sensitivity, detection limits, equilibrium constants, the ΔG, and ΔΔG were better for signal-on than signal-off. In an attempt to understand how thermodynamics played a role in the sensitivity and LOD/LOQ for signal-on vs. signal-off we looked to differences between the types of competitive binding reactions (Table 2 and Scheme 1B and 1C). Then the predicted Gibbs energy and the association constant of the binding equilibrium, $K_A = K_{eq}$, were used to determine how thermodynamic values and equilibrium concentrations might influence the sensitivity and LOD.

As depicted in Scheme 1 the MB and RQ have a stem-loop structure. As the loops of the hairpins interact with their respective targets the target must outcompete the stem stability. Figure 4 shows the predicted hairpin structures probability for RQ and MB. The MB has a typical stem-loop structure but the terminal A-T base pair was only predicted to bind 60-70 % of the time in 1 M Na$^+$ (and 25 % of the time in millimolar amounts of Na$^+$ and Mg^{++}, Figure S2). These probabilities may be underestimations given the LNA's, on the other hand the proximities of the dye-quencher pair causes unknown stability.
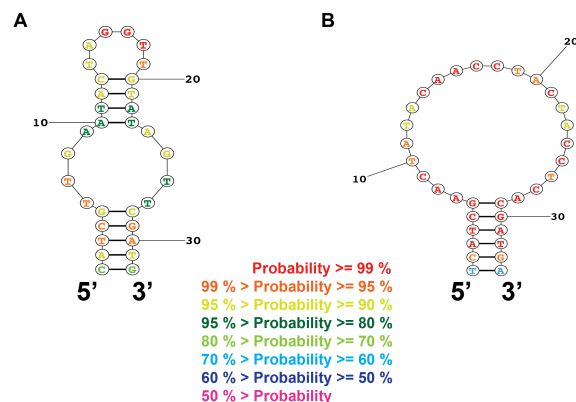

Figure 4. Structure probability prediction of the (A) RQ and (B) MB hairpins.[30] The probabilities indicate the likelihood that the interaction (bonded or un-bonded) shown will occur.

The competition reaction of the MB for let-7a is between a stem of 5-6 base pair interactions and loop-target complex with 22 base pair interactions. The RQ is predicted to have 5 base pairs, a 4x4 internal loop, another 4 base pairs, and a hairpin loop of 6 nucleotides, for a total of 9 base pairs. The RT and P must outcompete these 9 base pairs in order to bind the RQ to form 21 base pairs with RT and 11-13 base pairs with P. For the reporter-probe complex as a biosensor the competition reaction is between 11-13 base pair interactions of the (RQ+P) complex and 20 base pair interactions of the probe-target complex. In other words, the let-7a competes against a stem of 5-6 base pair interactions with the MB, but 11-13 base pairs with the reporter-probe complex.

Not all of the complementary interactions are predicted to

form base pairs in the (RQ+P) biosensor. The DINAMelt freeware[27-29] predicts that the (RQ+P) complex has up to 19 base pairs. However, only nine are predicted to occur from nucleotide 3 to 11 on the probe with over 99 % probability. The tenth and eleventh base pairs at probe positions 2 and 12 are predicted to form over 98 % and 94 % of the time, respectively. Both the twelfth and thirteenth base pairs at probe positions 1 and 13 are only predicted to occur 35 % to 50 % of the time, suggesting the binding events are dynamic. In fact, the base pair at probe position 13 may be more stable given the proximity to a LNA. The remaining base pair interactions are expected to occur less than 5 % of the time. Basically, half of the time there are 11 base pairs and the other half of the time there are 13 base pairs. Figure S3 of supplementary data shows the probability map and predicted structure of (RQ+P) binding interactions.[27–29] The dynamic nature of the nucleotides on the distal ends of the probe in the (RQ+P) biosensor most likely aid in the displacement reaction.

In the signal-off mechanism, the let-7a target must work against the stability of the (RQ+P) interaction. The $\Delta\Delta G$ between the (RQ+P) and the (P+let-7a) interaction is about -10 kcal/mol (see Table 3). The MB has a greater change in Gibbs energy, $\Delta\Delta G$ (- 23 kcal/mol), better sensitivity, and better LOD than the (RQ+P) biosensor. Taking this into consideration, one might wonder if the differences in $\Delta\Delta G$ influence the LOD and sensitivity for different recognition and transduction mechanisms.

To investigate the role of thermodynamics on the sensitivity and LOD we look to equilibrium concentrations derived from predicted Gibbs energy and the association constant of the binding equilibrium, K_A. The relationship between Gibbs energy and the K_A is given by the following equations:[31]

$$\Delta G = -RT\,ln(K_A) \tag{3}$$

$$K_A = e^{-\Delta G/RT} \tag{4}$$

where R is the ideal gas constant (1.987 x 10^{-3} kcal/mol•K) and T is the temperature (in Kelvin). For bimolecular interactions between single strands the K_A was obtained from solving equation 4 using the Gibbs energy from Figure 3. The K_A's were 2.3 x 10^{10}, 2.5 x 10^{17}, 9.9 x 10^{17}, and 8.3 x 10^{19} for (RQ+P), (RQ+RT), (P+let-7a), and (MB+let-7a), respectively. The equilibrium concentrations of (RQ+P), (RQ+RT), and (MB+let-7a) formed were determined from the initial reaction conditions prior to hybridization and the respective K_A value.

Using the K_A for (RQ+P), 1 μM RQ, and 500 nM P, only about 43 pM of P will be uncomplexed. Given our sensitivity, limit of detection, and noise at 500 nM (RQ+P), this amount is negligible. In other words essentially all probe is converted to (RQ+P). Similarly a negligible amount of let-7a, about 1.2 x 10^{-20} M, will be uncomplexed upon reaction with MB. The same can be found for (RQ+RT); only 4.0 x 10^{-18} M of RT will be uncomplexed. These results were expected from the predicted ΔG and K_A values.

The overall reaction and equilibrium constant (K_{comp}) that govern the competition reaction between (RQ+P) and (P+let-7a) are given by:

$$(RQ+P) + let\text{-}7a \leftrightharpoons (P+let\text{-}7a) + RQ \tag{5}$$
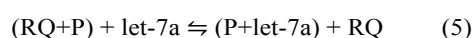
$$K_{comp} = \frac{[RQ][(P+let\text{-}7a)]}{[let\text{-}7a][(RQ+P)]} \tag{6}$$

Derivation of the equilibrium concentrations of (P+let-7a) and RQ from the reaction requires consideration of two competing reactions. We must simultaneously consider association of (P+let-7a) and the dissociation of the (RQ+P) complex as given by the following reactions and equilibrium constants:

$$P + let\text{-}7a \leftrightharpoons (P+let\text{-}7a) \tag{7}$$

$$(RQ+P) \leftrightharpoons P + RQ. \tag{8}$$
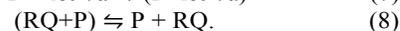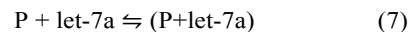
$$K_A^{(P+T)} = \frac{[(P+let\text{-}7a)]}{[P][let\text{-}7a]} \tag{9}$$

$$K_D^{RQ,P} = \frac{[(RQ)(P)]}{[(RQ+P)]} \tag{10}$$

where $K_D^{RQ,P}$ is the dissociation constant of (RQ+P) and $K_A^{(P+let7a)}$ is the association constant of (P+let7a). Using equations 9 and 10 we can rewrite equation 6 in terms of $K_D^{RQ,P}$ and $K_A^{(P+let7a)}$ as follows:

$$K_{comp} = \left(K_D^{RQ,P}\right)\left(K_A^{(P+let7a)}\right) \tag{11}$$

Equation 11 was used in the derivation of the quadratic equation to determine the change in equilibrium concentrations as (P+let-7a) complex forms and RQ is freed. First, the amount of (RQ+P) formed was determined using its K_A. Then we use the (RQ+P) equilibrium concentration and its dissociation constant $K_D^{RQ,P}$, the (P+let-7a) association constant $K_A^{(P+let7a)}$, and the amount of let-7a added to find the equilibrium concentrations of (P+let-7a) and RQ-hairpin.

Given the signal-off (RQ+P) biosensor had a limit of detection around 3 nM we used 0.1 nM of let-7a, which is lower than the signal-off limits of detection, to determine if thermodynamics alone define the limits of detection. If we find the reaction does not go to completion from a thermodynamic derivation, then there is a thermodynamic limitation on the LOD of the signal-off with (RQ+P). Recall that a mixture of 1 μM of RQ with 500 nM of P results in 43 pM of uncomplexed P and 499.957 nM of (RQ+P). For this calculation, 0.1 nM of let-7a was added to 499.957 nM (RQ+P) complex. From these initial conditions and the product of $K_D^{RQ,P}$ and $K_A^{P+let7a}$, we found about 0.1 nM of (P+let-7a) should form and only 5 x 10^{-22} M let-7a will be unreacted. Such a small amount compared to the nanomolar limits of detection is a negligible amount. In other words, we can say almost 100 % of let-7a reacts with P to form (P+let-7a). Thus from this standpoint thermodynamics should not influence the detection limits.

A similar approach can be used to determine if 0.02 nM of RT can be detected by the RQ. We pick a concentration below the empirical detection limit to see if thermodynamics alone will prevent the reaction from going to completion. Table 3 provides the K_A for the reaction of RQ and RT. The amount of (RQ+RT) formed is essentially 0.02 nM with 8.3 x 10^{-23} M of uncomplexed RT. Again thermodynamics alone is not influencing the detection limit.

There is a legitimate concern that uncomplexed probe will react with let-7a before interaction with the (RQ+P) complex. This will influence the accuracy of the measurement. Given only 42 pM of the probe is uncomplexed and the error in the LOD is only ± 1.3 nM, such a small loss of target will not ruin the accuracy of the signal-off (RQ+P) biosensor's measurement.

With excess RQ and considering the amount of predicted uncomplexed probe, the error associated with accuracy for the

LOD and LOQ are 1.5 and 0.5 %, respectively. An interesting result from this analysis is that as long as the uncomplexed probe is well below the LOD, then pico- to nanomolar limits of detection can still be reached. The upper limit of detection is defined by the amount of (RQ+P) actually formed.

Next we considered the equilibrium concentration of (RQ+P) prepared from solutions of 500 nM RQ and 500 nM P. The equilibrium concentrations were 495 nM (RQ+P), 5 nM (RQ), and 5 nM (P). Given the limits of detection, this amount of uncomplexed probe will be problematic. The thermodynamics will influence the accuracy and limit the dynamic range from about 5 nM to 495 nM. At the low end of the dynamic range, uncomplexed probe will bind to a significant amount of target before the (RQ+P) complex, thereby preventing accurate determination of the detection limit and ruining the overall accuracy.

From this analysis we find that as long as there is slight excess of RQ the amount of uncomplexed probe will not influence the sensitivity, limits of detection, or accuracy. Even the formation of (RQ+RT) is not influenced by thermodynamics, provided there is excess RQ. A similar argument can be made for the MB, provided MB has a greater concentration than its target.

If equimolar amounts of RQ and P are used, then the uncomplexed probe will be a limiting factor. However, it is not so much the thermodynamics alone that create this limitation but rather the respective initial concentrations of RQ and P. When using the reporter-probe biosensor for a given miRNA the amount of uncomplexed probe must be determined based on the amount of reporter and probe being used.

The more likely reason for the improved sensitivity and limit of detection for signal-on over signal-off is the amount of excess fluorescence from Cy5. We have shown that the sensitivity and LOD/LOQ of signal-off is better when there are fewer dye molecules in the probe volume. Signal-on also showed better sensitivity when the starting concentration of RQ was lower. Additionally, we have shown that lowering the concentration of the (RQ+P) biosensor lowers the limits of detection for signal-off. These results help give validity to the notion that detecting changes in fluorescence with a dimmer background leads to a more sensitive analysis. However, sensitivity is only one out of many metrics to consider. For miRNA detection in particular, selectivity is very important.

Another important consideration is the formation of MB and RQ homodimers (MB+MB) or (RQ+RQ) and their effect on the fluorescence. The RQ homodimer structure predicted by DINAMelt is 5 base pairs, a 4x4 internal loop, 4 base pairs, a 6x6 internal loop, 4 base pairs, a 4x4 internal loop, and 5 base pairs. The RQ homodimer structure still brings the 5' stems of each RQ molecule next to the 3' stems of the corresponding RQ molecule. Based on the homodimer structure, two dye-quencher pairs will form and the fluorescence results are not expected to deviate from RQ hairpin results. Any unquenched fluorescence from a homodimer will be as much as two hairpins. Even if an equilibrium between RQ homodimer and hairpin existed the ensemble nature of the measurement would average out the signal fluctuations over the acquisition time. The instrumental error of 0.02 % serves as evidence that any equilibrium between hairpin and homodimer does not affect any of the fluorescence results for RQ or MB.

The predicted ΔG and T_m values of the (RQ+RQ) homodimer are -6.4 kcal/mol and 18.5°C, respectively. Based on the melting temperature, the RQ homodimer should be unstable and not form at room temperature. The bimolecular RQ homodimer has a lower ΔG than the unimolecular hairpin, but the melting temperature for the homodimer is lower than the hairpin. These competing thermodynamic values make it difficult to determine the more thermodynamically stable species. In fact, these predicted values are likely underestimates given the use of LNA's throughout the reporter. Furthermore, the presence of quencher and dye may either stabilize or destabilize the predicted ΔG and T_m values. Any changes in stabilization should be similar for both hairpin and homodimer because they use the same LNA's and dye-quencher pairs. In the event the melting temperature is larger than expected and close to or greater than room temperature some RQ homodimer may form.

Even if RQ homodimers do form, once probe is added the (RQ+P) complex is more stable in all respects than the RQ homodimer resulting in disruption of any homodimers. Thus any freed RQ will contribute to the baseline as either a hairpin or form a new homodimer. Early experiments showed that addition of probe beyond equimolar amounts of probe to a fixed amount of RQ gave more signal but the slope changed and in some cases plateaued rapidly (data not shown). However, it was hard to distinguish sample preparation errors from homodimers in relation to this increase in signal. Future biosensor designs will investigate this issue in more detail.

DINAMelt assumes that the solution concentrations are dilute enough so the average distance between two interacting molecules is greater than the intramolecular distance needed for each molecule to sample all possible conformations.[27,29] This assumption coupled with the stability of the hairpin suggests the hairpin will form prior to the homodimer. This will be especially true upon RQ displacement from the probe when miRNA is added. Zuker and co-workers[27,29] never state what dilute means; however, they use solutions that contain DNA concentrations in the hundreds of micromolar to validate their energy predications with experiments. Given the reporter stock solutions used in this study are hundreds of micromolar and our operation concentrations are nano- to low micromolar, the RQ solutions are sufficiently dilute that the hairpins should form first.

To estimate the amount of RQ homodimer that may form we considered two cases: (1) homodimer from open RQ that is in equilibrium with the closed conformation and (2) homodimer formation if the homodimer forms prior to hairpin. First the amount of open RQ was determined from the Quickfold function to obtain Gibbs energy of hairpin formation. In a solution of 1µM RQ, only 2.6 nM RQ will be in the open conformation. This open conformation will more likely form a homodimer than the closed conformation. Considering two strands are needed to form a homodimer, the homodimer equilibrium constant, and a total open RQ concentration of 2.6 nM; only 93 fM of RQ homodimer will form. Next we calculated the equilibrium concentration of RQ homodimer using 1 µM and 500 nM RQ as the total initial concentrations and assumed the homodimer forms first. The equilibrium RQ homodimer concentrations are 13 nM and 3.3 nM for 1 µM and 500 nM RQ, respectively. From this analysis RQ homodimers do not predominantly form because they make up about 0 to 1.3 % of the RQ solution depending on the total amount of RQ present. These values are subject to debate because LNA's provide additional stability and the dye-quencher pair influences the energy in unpredictable ways. From these calculations we expect any where between 93 fM and 13 nM of RQ homodimer for 1 µM RQ. The extent of the RQ homodimer

will be tested in future work using a mixture of RQ strands with and without the dyes or quenchers.

For comparison we investigated the homodimer of the molecular beacon. From Quickfold a solution of 1 µM MB will have about 0.8 nM in the open conformation. The Gibbs energy and melting temperature for a MB homodimer is -7.7 kcal/mol and 19.5 °C, respectively. These values imply the MB homodimer is as stable or more stable than the RQ homodimer. Considering just the amount of open MB, about 80 fM of MB will form a homodimer. If we assume the MB forms a homodimer prior to a hairpin, then the equilibrium concentrations of homodimers are 86 nM and 25 nM for initial concentrations of 1 µM and 500 nM MB respectively. MB homodimer formation ranges from 80 fM to 86 nM for 1 µM total MB.

The main difference between RQ and MB hairpins and homodimers is the predicted structure and associated probability of base pair formation. Supplementary Figure S2 compares probabilities of RQ and MB hairpins and homodimers. For the MB the DINAMelt[27-29] partition function predicts a homodimer structure of 5 base pairs, a 22x22 internal loop, and 5 base pairs. The probability of MB homodimer formation is less than 64 % of the time. The hairpin on the other hand is predicted to have a 5 base pair stem over 97 % of the time, but the 6th base pair in the stem is only expected to occur less than 25 % of the time and is even less likely than the other 5 base pairs of the stem (note these values are in contrast to Figure 4 because DINAMelt lets you define the actual salt concentration). The MB hairpin structure is 5 to 6 base pairs and a hairpin loop of 22 nucleotides. In other words, the probability of homodimer formation is less than that of the hairpin (Figure S2). On the other hand, the probability of forming an RQ hairpin structure over a homodimer is about the same. This supports the argument that an equilibrium may exist between hairpins and homodimers. However, the very small instrumental error does not support the claim that the equilibrium will influence all of the fluorescence results.

Selectivity

Selectivity of the MB and (RQ+P) biosensors were investigated using a three-nucleotide variation of the let-7a sequence. Table 1 shows the sequence for let-7a and the let-7a variant (let-7aV). The selectivity was determined by the amount of signal change that each oligonucleotide caused when added to equimolar amounts of (RQ+P) or MB (both at 500 nM). Recall the only difference in the nucleic acids used for reporting molecules (RQ and MB) were the sequence in the loop region and an extra terminal A-T base pair on the MB. This extra base pair in the stem was to improve stability in an attempt to prevent non-selective binding. The stems used on the MB were adapted from Bao's work on dual molecular beacons.[32]

As seen in Figure 5, the MB had about a 17-fold increase in signal when complexed with either let-7a or let-7aV. This shows the MB was susceptible to non-selective binding when just 3 nucleic acid residues in the target were changed.

Addition of let-7a to the (RQ+P) complex causes the signal to decrease by a factor of 12.00 ± 0.029 fold (Figure 5). The (RQ+P) only showed a marginal decrease in signal by a factor of 1.080 ± 0.003 when let-7aV was added to (RQ+P) complex. A signal change factor of 1 represents the absence of non-selective binding. Thus very little non-selective binding occurred for the (RQ+P) biosensor.
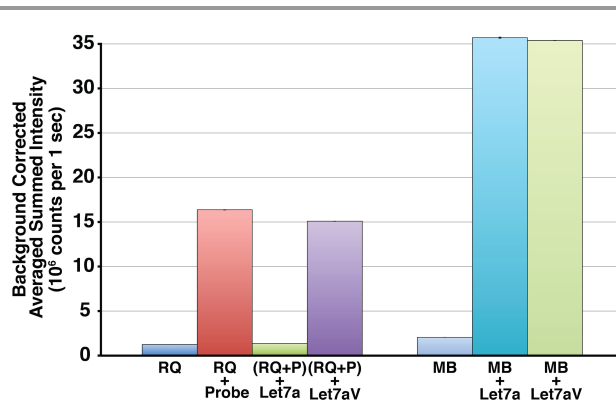

Figure 5. Selectivity of (RQ+P) and MB biosensors for let-7a and let-7aV. The (RQ+P) demonstrates significantly more selectivity than the MB for Let-7a. All reagents are 500 nM. Data bars represent background corrected and averaged peak summed intensities (N = 3). Error bars are too small to be seen.

The reason for the poor selectivity of the MB could be due to the fact that the stem of the MB only has three pairs of G-C interactions. To address problems with selectivity more G-C content could be added to the stem. However, using a MB developed by Akin and co-workers[33] for the 271–293 region of Sensorin mRNA with a stem of 6 G-C base pairs we were unable to detect the analyte, let alone any off-target interactions. The backbone of the loop and stem consisted of 2' O-methyloligoribonucleotide modifications. Such a modification increases stability and minimizes enzymatic degradation. However, adding more stable G-C content and stabilizing chemical modifications did not help improve the selectivity; rather it rendered the MB non-functional. (data not shown)

The change in thermodynamics of the MB for let-7a and let-7aV helps explain why the MB is not selective for let-7a alone. Recall from Table 3 (MB+let-7a) is more stable than the MB hairpin by almost 23 kcal/mol ($\Delta\Delta G$) and 7 °C (ΔT_m). The MB will also bind let-7aV because the (MB+let-7aV) interaction is more stable than the MB hairpin by nearly 12 kcal/mol ($\Delta\Delta G$) but the change in melting temperature is destabilized by about 13 °C ($+\Delta Tm$). Despite the destabilizing change in melting temperature the MB still binds the let-7aV. This suggests Gibbs energy contributes more to shifting the equilibrium than the melting temperature. In fact these are just two of many thermodynamic considerations. In future studies we plan to investigate the role of activation barrier, enthalpic, and entropic regulation of the equilibrium.

The high selectivity of the (RQ+P) biosensor for let-7a is due to the increased stability of the (RQ+P) complex compared to the stability of the MB's hairpin conformation. The biosensor was selective towards the let-7a target since the (P+let-7a) formation is more stable than the (RQ+P) complex by 10 kcal/mol ($\Delta\Delta G$) and 16 °C (T_m) (see Table 3). In comparison, this was not the case for (P+let-7aV). Figure 1 shows (P+let-7aV) interaction was less stable than the (RQ+P) complex by 0.3 kcal/mol and had a T_m that is 4 °C lower than the (RQ+P) complex. These are both destabilizing changes. In the presence of let-7aV, there was no sufficient thermodynamic driving force to disrupt the (RQ+P) complex.

From Figure 5 we can also see the signal from the MB hairpin is larger than the RQ hairpin. Despite the fact RQ and MB have nearly identical stems (MB has an additional terminal A-T base pair), their loop sequences are different and contribute to different ΔG and K_A values for their respective hairpins. The MB hairpin is about 1 kcal/mol more stable than the RQ

hairpin. Using 500 nM of MB and RQ and their respective K_A values, we found that about 0.4 nM of MB and about 1.3 nM of RQ will be in an open conformation. Taking this information into consideration the MB should actually have a lower signal than RQ, but this was not observed. One reason for the intensity difference is Guanine tends to quench fluorescence better than any other nucleic acid.[1] The RQ has the Cy5 much closer to a terminal Guanine than the MB. The other reason is related to the predicted structure of the MB. Figure 4 shows the terminal A-T base pair is only formed 60 to 70 % of the time. Thus the stem of the MB fluctuates by opening and closing more than the RQ. During the acquisition time the average signal is slightly higher for MB than RQ due to the Cy5 and Q fluctuation. Figure S4 in the supplementary section compares signal intensity from equimolar amounts of RQ to MB. Equilibrium between MB homodimer and hairpin may be another explanation for MB having more intensity than the same amount of RQ. Based on DINAMelt's Energy Minimization model the MB homodimer only has 5 base pairs formed by the complementary stems and leaves the remaining nucleotides unbound. Such a structure only forms one pair of dye-quencher. The other pair may interact from time to time, but overall will have an increased fluorescence if they are not quenched or quenched to a lesser extent. Of course an even more simple reason for the slight difference is sample preparation and cuvette placement errors. However, such simple errors do not explain the consistently greater signal observed with MB over RQ.

Another interesting observation is that the RQ biosensor exhibited less change in signal upon binding to P and RT than the MB biosensor did upon binding to let-7a. Given the fact Cy5 and the quencher are the same for RQ and MB the signal change should have been the same. Considering the type of quenching and examination of the secondary structure of the (RQ+P) and the (MB+let-7a) complexes reveals a plausible explanation for the difference in signal change (Figure S5). Given the lack of full complementarity of the probe for RQ, the secondary structure of the (RQ+P) complex may have the quencher and Cy5 closer together than in the case of (MB+let-7a). This is plausible because of the noncomplementary section of the reporter allowing the Cy5 to fold back closer to the quencher. From a FRET quenching standpoint this would explain the smaller change in signal of RQ compared to MB. In addition, the Cy5 dye could orient itself in such a way as to interact with the nucleotides on the RQ or in the non-complementary region of the probe leading to increased signal quenching.[1]

The evidence of distance dependence between Cy5 and quencher is further evident by comparison of intensities of (RQ+P), (RQ+RT), and (MB+let-7a) in Figure 1. In the case of RQ for P or RT, the RT binding gives a larger change in signal. Considering the fully complementary nature of (RQ+RT) binding, a larger distance between the quencher and Cy5 is expected. In addition, there will be fewer degrees of freedom for Cy5 meaning it will be less likely to interact with nucleotides and thus less quenching is expected.

As for the difference in signal between (RQ+RT) and (MB+let-7a), the MB is simply longer than the RQ by 2 bases. When the distance between Cy5 and quencher is extended by target binding, the MB will be longer than RQ and thus the distance between quencher and Cy5 will be greater leading to less quenching. The argument about Guanine quenching can also be used here as RQ has Cy5 closer to a terminal Guanine than in the case of MB. These arguments make more sense and

seem more convincing from a FRET, dynamic, or static quenching standpoint when you consider the likelihood of interaction between quencher and Cy5.

Signal to Noise Comparison

The average signal-to-noise ratio (S/N) from three cuvette placements is presented in Figure 6. The S/N was evaluated at a single data point, 673 nm. The reason for this was to get an idea of the S/N at a given wavelength over time. We found no statistically significant difference in the S/N between the signal-on and -off mechanisms (95 % confidence level).
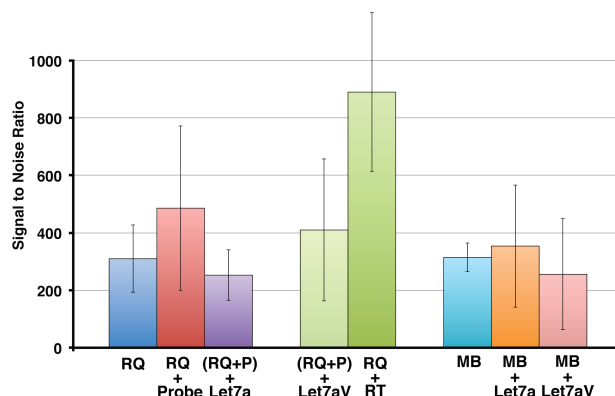

Figure 6. Average Signal to Noise (S/N) ratio for various combinations of RQ and MB with probe, RT, let-7a, and let-7aV. S/N was statistically similar for both signal-on and signal-off mechanisms. All reagents were 500 nM, (N = 3).

While the error in S/N is rather large, inspection of the actual emission plots show the signal is quite reproducible within one cuvette placement (Figure S6). The error in the average S/N arises from cuvette placement error (Figure S7).

On a fundamental level the ability to observe a change in signal should be limited by the accompanied noise. The argument that if the S/N of signal-on is the same as signal-off, then the sensitivity should be the same is not entirely true based on the data presented above. The sensitivities were actually quite similar with signal-on being only twice as sensitive as signal-off. However, the LOD for signal-on was about 20 times better than that of signal-off.

Variability of the Signal-off Method

We investigated the signal reproducibility of the (RQ+P) biosensor in terms of instrumental error, cuvette placement error, and sample preparation method. Instrumental error was determined for signal-off experiments by examining the RSD for six acquisitions within 1 cuvette placement (N = 6). Cuvette placement error was determined from the RSD of the three cuvette placements, or 18 total frames (N = 6, N' = 3, 6x3 = 18).

The signal from a 500 nM solution of (RQ+P) was determined by summing over a region of interest (640.1425 to 690.0957 nm). The RSD of the signal from three cuvette placements was about 2%. The instrumental error was determined to be 0.02% RSD from six acquisitions within one cuvette placement. Note that the error in S/N discussed in the previous section arises from looking at a single data point, while here the RSD accounts for intensity summed over the region of interest.

The reproducibility of the (RQ+P) biosensor from solution preparation for the calibration curves was tested for intra- and

inter-assay variability. Inter-assay variability was used to determine the day-to-day variation when solutions were prepared separately on different days. Intra-assay variability determined the variation when solutions were prepared on one occasion but the experiments were run on three separate days. The details of how the solutions were prepared can be found in the experimental section above.

Table 4 shows the slopes and RSD of the slopes for intra- and inter-assay variability were nearly identical at $\sim 3.7 \times 10^4$ counts/nM and 12 %, respectively. The LOD for inter- and intra-assay variability were 3.30 ± 0.40 and 1.12 ± 0.14 nM. The RSD for the LODs from each type of variability were also about 12 %. Not only did this show the sensitivity and LODs of the (RQ+P) biosensor had good reproducibility, but also the way the sample was prepared did not change the outcome of the

Table 4. Inter- and Intra-assay Variability for Signal-off

	Inter- Assay	Intra- Assay
Average Slope (counts/nM)	-37526	-37804
Standard Deviation Slope (counts/nM)	4516	4599
RSD Slope	12.0 %	12.2 %

N = 3 for inter- and intra-assay variability

experiment.

Advantages and Challenges of Signal-on and Signal-off Methods for Future Cell and Tissue Imaging

The sensing application will greatly dictate the analytical FOM and ultimately the biosensor that will demonstrate optimal performance. The body of work presented herein only dealt with analysis in clean solutions. Future work will revisit analysis of signal-on vs. signal-off in more complex cell and tissue samples.

Currently the reporter-probe biosensor functions in signal-off mode but preliminary data that will be the subject of future work shows we can use donor-acceptor dye pairs for FRET enhancement. The signal-off and signal-on reporter-probe biosensor will find most use as an *in situ* sensor for cell and tissue imaging. The primary advantage of the reporter-probe biosensor design is for measuring low copy number and small changes in miRNA expression when other sensors cannot provide enough sensitivity or specificity. With tissue and cellular analysis, endogenous autofluorescence, off-target binding, and enzymatic degradation may raise the noise floor and mask any signal from small amounts or changes of miRNA.[34] Molecular beacons are notorious for burying signal from miRNA in the background because of sensor degradation from enzymes.[1,2,32] Thus, the reporter-probe biosensor may prove more useful because of its reduced false signals,[1] high sensitivity, high S/N, and high selectivity.

One advantage to the signal-off sensor is its baseline signal will be well above the background signal established by autofluorescence of the cell or tissue. The reporter-probe biosensor may have a better chance to detect a decrease in fluorescence from the dye's baseline rather than an increase from the baseline of cells and tissues established by autofluoresence.

Signal-off biosensors serve best to test for the absence of a given miRNA that regulate oncogenes. For example, let-7a regulates the expression of oncogenes like RAS and MYC.[6]

Loss of let-7a will allow RAS and MYC messenger-RNA and subsequent proteins to become over expressed and can lead to cancer.[6] In this case a sensitive signal-off sensor is needed to report on the absence or decrease of miRNA that regulate oncogene expression.

Limitations for both signal-on and signal-off biosensors for *in situ* cell and tissue imaging include the difficulty of transfection,[32] quantification of copy number,[34–38] and determination of miRNA location.[34] Often the variability from cell-line to cell-line requires trying different types of transfection techniques to find the most efficient one.[32] Once the appropriate transfection technique is found, ensuring the uptake of biosensors is the same or similar among all the cells under investigation remains a challenge.

Use of the reporter-probe biosensor for cell and tissue imaging will require hybridization of the reporter and probe prior to transfection into the cells or tissue. If the reporter and probe are transfected individually, then the fluorescence intensities in different cells will vary and the probe will most likely bind the miRNA before the reporter. If the reporter-probe complex is not formed first, then it will be very difficult to monitor signal change before and after a biochemical change.

Both signal-on and signal-off techniques will require a standard curve for *in situ* quantification of miRNA copy number.[34,37] Positive and negative control cells or tissues are always required to validate quantification results. In general, both signal-on and signal-off biosensors for *in situ* cell and tissue imaging is qualitative or semi-quantitative at best.[35–38] Determination of miRNA copy number is especially difficult given their small size and low expression.[39] In some cases there are discrepancies between different types of *in situ* methods and quantitative real time polymerase chain reaction (qRT-PCR) or microarray quantification of messenger-RNA, gene transcript, and especially miRNA.[35,40] There are a few examples of ensemble and single molecule *in situ* biosensors that give messenger-RNA copy numbers that correlate well with qRT-PCR and other *in situ* analysis techniques but not many for miRNA copy number.[10,34,37]

Counting miRNA copy number by measuring fluorescence from a diffraction limited spot in cell and tissue imaging may be difficult if more than one miRNA or even one reporter molecule is present in the probe volume.[34] One difficulty of measuring copy number in living cells will be the diffusion of the biosensor for both signal-on and signal-off during the acquisition time. Basically if the biosensor drifts back into the detection volume you will count the same miRNA at least twice, this is especially problematic for single molecule *in situ* analysis.[41] Alternatively for ensemble measurements if many biosensors diffuse into and out of the detection volume during acquisition, then the intensity from one spot may correlate with many molecules rather than just one. Even fixed cells will have problems with quantification because signal-on sensors that generate fluorescence from a single spot may come from a single copy if the miRNA are dispersed throughout the cell or from many copies if they are co-localized.[34] Considerations of the cell's volume, miRNA copy number, and the diffraction limitation of the objective are needed for any quantitation or counting of fluorescent spots. In addition to following calibrations similar to work done by Femino *et al.*,[42] we will investigate standard addition with mock miRNA for quantification with the signal-off reporter-probe biosensor.

Determination of miRNA location will be the most challenging aspect for signal-off biosensors. Location information is particularly important because miRNA in one

cell type may have a different role in another cell type.[6,36] It is conceivable that signal-off sensing could still permit location and determination of copy number by counting dark spots. Tsourkas and co-workers describe a method to find bright spots from messenger-RNA biosensors by sampling dim intensity around the bright spot to define the size of the bright spot for subsequent counting.[37] Signal-off could perform the opposite task of searching for dim spots by sampling around the dim spot to find where it gets brighter thus defining a dim spot. Alternatively a negative image could be made that transforms bright signals into dark ones and dark signals into bright ones. Then a method similar to that described by Tsourkas could be used to gain location information and possibly copy number of miRNA.[37]

We aim to use about 1 nM of a reporter-probe biosensor in about 1 pL of cellular volume. This corresponds to about 600 biosensors. Just like signal-on generates signal from binding to a miRNA, so too can the signal from a reporter be correlated to a single probe. If the number of spots in control and altered cells are counted and compared, then the number of miRNA can be determined by subtracting the number of bright spots in the control from altered cells. Future designs will investigate methods to incorporate an internal standard to the sensor to account for inherent variability of quantification by comparison to controls.

Following fluorescent spots in cells for tracking the transportation of miRNA will only work if the miRNA is chemically modified with a dye and incorporated in the RNA-induced silencing complex (RISC).[43] Performing *in situ* labeling is difficult and may actually change the nature of the miRNA. Monitoring location and even transport of miRNA in cells using molecular beacons, reporter-probes, or even ratiometric biomolecular beacons[37] will not be very informative and any results will be suspect.[34] These types of sensors are best for location information in tissue to identify the cells that show altered expression of miRNA indicative of disease. The reason miRNA biosensors that bind directly to the miRNA preclude tracking is once the sensor binds the miRNA it becomes non-functional and can no longer participate in regulation of messenger-RNA. Furthermore the miRNA bound biosensor complex or biosensor itself can diffuse any where in the cell and its location may be meaningless. The most important location information comes from cell specific location information from tissue imaging.

Conclusions

Taking these results in the aggregate, we have quantifiable data to show that there is only a small difference between signal-on and signal-off in terms of LOD and sensitivity. The LOD for signal-on was a little over an order of magnitude (20-30 times) better than signal-off. However, by adjusting the concentration of the (RQ+P) biosensor we showed both signal-on and signal-off can detect miRNA down to 50 – 200 pM. In terms of sensitivity and reproducibility signal-on and signal-off were comparable. The reproducibility did vary based on cuvette placement error. The cuvette error defined the reproducibility rather than the biosensor itself.

The idea that LOD is better for signal-on than signal-off due to the difficulty in sensing a signal decrease against a bright background is true to an extent. We observed improved sensitivity by lowering the concentration of RQ and (RQ+P). In addition, lowering the (RQ+P) complex concentration lowered the LOD for signal-off from nanomolar to picomolar. Using

less (RQ+P) gave a dimmer background, permitting smaller changes in signal to be observed. Finally, we demonstrated that the S/N was the same for signal-on and signal-off.

Analysis of how thermodynamics influences the equilibrium concentrations revealed that a slight excess of RQ was needed to ensure any uncomplexed probe did not influence the sensitivity, limits of detection, or accuracy. However, if equimolar amounts of RQ and P were used, then the uncomplexed probe will be a limiting factor. This means for a given (RQ+P) biosensor the amount of excess RQ needs to be determined such that it will not influence the accuracy but minimize unnecessary background signal.

Sensitivity and LOD are important analytical FOMs for determining the performance of a fluorescent biosensor, but other analytical FOM play a role in determining the overall performance of a biosensor. The signal-off (RQ+P) biosensor proved to be significantly more selective than the MB for the same analyte. However, the advantage is in the recognition mechanism rather than the transduction mechanism. Future generation biosensor designs will focus on FRET enhancement to combine the attributes of signal-on sensitivity with our displacement mechanism to improve sensitivity, selectivity, reproducibility, and reduce false signals.

Notes and references

[a] 153 Gilbert Hall, Corvallis, OR 97331, United States of America

Email: Sean.Burrows@oregonstate.edu

1 N. E. Larkey, C. K. Almlie, V. Tran, M. Egan and S. M. Burrows, *Anal. Chem.*, 2014, **86**, 1853–1863.

2 J. B. Sternberg and N. A. Pierce, *Nano Lett.*, 2014, **14**, 4568–4572.

3 J. R. Buchan and R. Parker, *Science*, 2007, **318**, 1877–1878.

4 D. P. Bartel, *cell*, 2004, **116**, 281–297.

5 B. N. Johnson and R. Mutharasan, *The Analyst*, 2014, **139**, 1576.

6 C. M. Croce, *Nat. Rev. Genet.*, 2009, **10**, 704–714.

7 M. Schäferling and S. Nagl, *Anal. Bioanal. Chem.*, 2006, **385**, 500–517.

8 P. J. Santangelo, *Nucleic Acids Res.*, 2004, **32**, e57–e57.

9 E. G. Matveeva, Z. Gryczynski, D. R. Stewart and I. Gryczynski, *J. Lumin.*, 2010, **130**, 698–702.

10 A. E. Prigodich, P. S. Randeria, W. E. Briley, N. J. Kim, W. L. Daniel, D. A. Giljohann and C. A. Mirkin, *Anal. Chem.*, 2012, **84**, 2062–2066.

11 S. R. Ryoo, J. Lee, J. Yeo, H. K. Na, Y. K. Kim, H. Jang, J. H. Lee, S. W. Han, Y. Lee, V. N. Kim and D. H. Min, *ACS Nano*, 2013, **7**, 5882–5891.

12 D. S. Seferos, D. A. Giljohann, H. D. Hill, A. E. Prigodich and C. A. Mirkin, *J. Am. Chem. Soc.*, 2007, **129**, 15477–15479.

13 S. Su, J. Fan, B. Xue, L. Yuwen, X. Liu, D. Pan, C. Fan and L. Wang, *ACS Appl. Mater. Interfaces*, 2014, **6**, 1152–1157.

14 X. Xia, Y. Hao, S. Hu and J. Wang, *Biosens. Bioelectron.*, 2014, **51**, 36–39.

15 H. Dong, J. Zhang, H. Ju, H. Lu, S. Wang, S. Jin, K. Hao, H. Du and X. Zhang, *Anal. Chem.*, 2012, **84**, 4587–4593.

16 P. Shah, P. W. Thulstrup, S. K. Cho, Y. J. Bhang, J. C. Ahn, S. W. Choi, M. J. Bjerrum and S. W. Yang, *The Analyst*, 2014, **139**, 2158.

17 W. J. Kang, Y. L. Cho, J. R. Chae, J. D. Lee, B. A. Ali, A. A. Al-Khedhairy, C. H. Lee and S. Kim, *Biomaterials*, 2012, **33**, 6430–6437.

18 B. Dubertret, M. Calame and A. J. Libchaber, *Nat. Biotechnol.*, 2001, **19**, 365–370.

19 A. P. Silverman and E. T. Kool, *Chem. Rev.*, 2006, **106**, 3775–3789.

20 H. J. Tanke, R. W. Dirks and T. Raap, *Curr. Opin. Biotechnol.*, 2005, **16**, 49–54.

21 J. Guo, J. Ju and N. J. Turro, *Anal. Bioanal. Chem.*, 2012, **402**, 3115–3125.

22 A. Shibata, H. Abe and Y. Ito, *Molecules*, 2012, **17**, 2446–2463.

23 D. Harris, in *Quantitative Chemical Analysis*, W. H. Freeman and Company, New York, NY, 8th edn., 2010, p. 408.

24 H. Du, C. M. Strohsahl, J. Camera, B. L. Miller and T. D. Krauss, *J. Am. Chem. Soc.*, 2005, **127**, 7932–7940.

25 J. Liu, Z. Guan, Z. Lv, X. Jiang, S. Yang and A. Chen, *Biosens. Bioelectron.*, 2014, **52**, 265–270.

26 P. B. Landon, S. Ramachandran, A. Gillman, T. Gidron, D. Yoon and R. Lal, *Langmuir*, 2012, **28**, 534–540.

27 N. R. Markham and M. Zuker, *Nucleic Acids Res.*, 2005, **33**, W577–W581.

28 N. R. Markham and Zuker, Michael, in *Bioinformatics, Volume II*, Humana Press, 2008, vol. 453, pp. 3–31.

29 R. A. Dimitrov and M. Zuker, *Biophys. J.*, 2004, **87**, 215–226.

30 J. S. Reuter and D. H. Mathews, *BMC Bioinformatics*, 2010, **11**, 129.

31 N. L. Craig, O. Cohen-Fix, R. Green, C. Greider, G. Storz and C. Wolberger, in *Molecular biology: principles of genome function*, Oxford University Press, Oxford ; New York, 1st edn., 2010, p. 93.

32 P. Santangelo, N. Nitin and G. Bao, *Ann. Biomed. Eng.*, 2006, **34**, 39–50.

33 S. Jockusch, A. A. Martí, N. J. Turro, Z. Li, X. Li, J. Ju, N. Stevens and D. L. Akins, *Photochem. Photobiol. Sci.*, 2006, **5**, 493.

34 S. Pitchiaya, L. A. Heinicke, T. C. Custer and N. G. Walter, *Chem. Rev.*, 2014, **114**, 3224–3265.

35 J. Hanna, H. Wimberly, S. Kumar, F. Slack, S. Agarwal and D. Rimm, *BioTechniques*, 2012, **52**.

36 L. F. Sempere, *Expert Rev. Mol. Diagn.*, 2014, **14**, 853–869.

37 X. Zhang, Y. Song, A. Y. Shah, V. Lekova, A. Raj, L. Huang, M. A. Behlke and A. Tsourkas, *Nucleic Acids Res.*, 2013, **41**, e152–e152.

38 M. de Planell-Saguer and M. C. Rodicio, *Clin. Biochem.*, 2013, **46**, 869–878.

39 S. Basu and C. Sachidanandan, *Chem. Rev.*, 2013, **113**, 7952–7980.

40 J. Sano and K. H. Kato, *Zoolog. Sci.*, 2009, **26**, 745–753.

41 S. M. Burrows, R. D. Reif and D. Pappas, *Anal. Chim. Acta*, 2007, **598**, 135–142.

42 A. M. Femino, F. S. Fay, K. Fogarty and R. H. Singer, *Science*, 1998, **280**, 585–589.

43 S. Pitchiaya, J. R. Androsavich and N. G. Walter, *EMBO Rep.*, 2012, **13**, 709–715.